Architecturally Induced Multiresponsive Vesicles from Well-Defined Polypeptides. Formation of Gene Vehicles

9 AUTHORS, INCLUDING:

Hermis Iatrou
National and Kapodistrian University of Athens
123 PUBLICATIONS **5,957** CITATIONS

H. Frielinghaus
Forschungszentrum Jülich
137 PUBLICATIONS **1,407** CITATIONS

Janne Ruokolainen
Aalto University
214 PUBLICATIONS **6,482** CITATIONS

Hadjichristidis Nikos
King Abdullah University of Science and Tech…
301 PUBLICATIONS **8,815** CITATIONS

Architecturally Induced Multiresponsive Vesicles from Well-Defined Polypeptides. Formation of Gene Vehicles

Hermis Iatrou,*,† Henrich Frielinghaus,‡ Sirkku Hanski,§ Nikos Ferderigos,†
Janne Ruokolainen,§ Olli Ikkala,§ Dieter Richter,‡ Jimmy Mays,⊥,# and
Nikos Hadjichristidis*,†

Chemistry Department, University of Athens, Panepistimiopolis Zografou, 15771, Athens, Greece, Institut für Festkörperforschung, Forschungszentrum Jülich GmbH, D-52425 Jülich, Germany, Helsinki University of Technology, P.O. Box 2200, FIN-02015 HUT, Espoo, Finland, Chemistry Department, University of Tennessee at Knoxville, Knoxville, Tennessee 37996, and Center for Nanophase Materials Sciences, Oak Ridge National Laboratory, Oak Ridge, Tennessee 37831

Received April 1, 2007; Revised Manuscript Received April 24, 2007

A series of novel, partially labeled amphiphilic triblock copolypeptides, PLL-*b*-PBLG-d7-*b*-PLL, has been synthesized, where PLL and PBLG-d7 are poly(L-lysine hydrochloride) and poly(γ-benzyl-d7-L-glutamate), respectively. The synthetic approach involved the sequential ring-opening polymerization (ROP) of γ-benzyl-L-glutamate and ε-Boc-L-lysine *N*-carboxy anhydrides by a diamino initiator using high-vacuum techniques, followed by the selective deprotection of the Boc groups. Combined characterization results showed that the copolypeptides exhibit high degrees of molecular and compositional homogeneity. The synthesized copolypeptides had similar molecular weights, while the composition of the middle block ranged between 19 and 74% with respect to the monomeric units. Due to the macromolecular architecture of the copolypeptide and the rigid nature of the middle block, the formation of monolayers was favored, and, surprisingly, vesicles were formed in water at neutral pH over the entire compositional range. The vesicular structures were extensively characterized by static and dynamic light scattering, small-angle neutron scattering, atomic force microscopy, cryo-transmission electron microscopy, scanning electron microscopy, UV and Fourier transform infrared spectroscopy, and circular dichroism. In contrast to other vesicular structures derived from conventional polymers, the formed polypeptidic vesicles possess the unique feature of being stimuli-responsive to pH and temperature. When the copolypeptides were mixed with plasmid DNA (pDNA), large vesicular structures were also formed. The molecular characterization of the vectors was performed with most of the methods mentioned above, and indicated that the pDNA is both partially condensed on the PLL phase and partially encapsulated inside the vesicle. Consequently, the synthesized vectors combine the advantages of the polylysine−DNA systems to condense large amounts of genes, as well as those of the liposome−DNA systems to better protect the encapsulated DNA. These vectors are expected to present better gene transfection efficiency to the cell nucleus.

Introduction

Membranes and vesicular structures are the main components of the basic building blocks of living creatures, the cells. Vesicles are closed bilayers with a thickness of only a few nanometers[1] and play a critical role as nanocontainers to transport or protect several cellular components. Although phospholipids are the main building blocks for the formation of cellular and other vesicular membranes, amphiphilic macromolecules have attracted much attention since they have properties that can extend the chemical and physical limits of liposomes.[2,3] Consequently, the synthesis of well-defined amphiphilic materials capable of forming vesicles in water with tunable molecular characteristics is expected to boost biological applications such as drug and gene delivery.[4,5] Among them, polypeptides are the most promising materials since they self-assemble into hierarchically organized three-dimensional (3D) structures that can mimic natural proteins. This property is the most significant advantage over the conventional synthetic polymeric materials.

A few reports on polymer vesicles in water from conventional[6,7] or hybrid diblock copolymers,[8,9] as well as amphiphilic diblock copolypeptides[10−13] have been published. In most of these reports, a series of amphiphilic diblock copolymers with different compositions was synthesized; however, the formation of vesicular structures was limited only to a very small compositional window. It is our opinion that this is due to the conformational barrier of the architecture of the diblock copolypeptides, where an antiparallel orientation is required for the insoluble block in order to form the bilayer of the vesicle.

We reasoned that triblock copolypeptides of the ABA type, where A is a charged hydrophilic block and B is a rodlike hydrophobic block, could overcome the architecturally induced barriers of the diblock copolymers. An ABA copolypeptide can be considered as two A(B/2) diblock copolypeptides having an antiparallel orientation, connected on the chain end of the B block with a chemical bond. Therefore, due to the macromolecular architecture, an ABA copolypeptide would easily form a monolayer membrane similar to the bilayer formed by the diblock copolypeptides, simply by the self-assembly of the

* Corresponding author. Address: Chemistry Department, University of Athens, Panepistimiopolis Zografou, Athens, 15771, Greece. Tel: +30 210 7274330. Fax: +30 210 7221800. E-mail: hadjichristidis@chem.uoa.gr (N.H.), iatrou@chem.uoa.gr (H.I.).
† University of Athens.
‡ Forschungszentrum Jülich GmbH.
§ Helsinki University of Technology.
⊥ University of Tennessee at Knoxville.
Oak Ridge National Laboratory.

Table 1. Molecular Characteristics of the Triblock Copolypeptides PBLL-PBLG-d7-PBLL

sample	M_n PBLG-d7 $\times 10^3$	Total M_n $\times 10^3$	I (M_w/M_n)	M_n PBLL/2 $\times 10^3$	M_n total deprotected $\times 10^3$	% PBLG-d7 per monomeric unit
$L_{134}G_{64}L_{134}$	14.4	75.8	1.14	30.6	58.2	19.3
$L_{131}G_{137}L_{131}$	31.0	91.0	1.16	29.9	74.0	34.3
$L_{64}G_{181}L_{64}$	67.4	91.6	1.15	12.1	84.7	73.7

insoluble middle block. Moreover, the rigid nature of the middle block would prevent the formation of the conventional core−shell micelle, since the molecule would not be able to bend.

In the past decade, DNA-based drugs have been developed for a wide range of human disorders. One of the significant advantages of these therapeutics over the low molecular weight pharmaceuticals is their tremendous specificity of action and lack of side effects associated with conventional drugs. The transfer of DNA across cellular barriers is very difficult, thereby preserving genomic information and preventing genetic contamination. By using vesicular structures and proteins that recognize cell surface receptors, viruses have the ability to overcome the intra- and extracellular barriers and deliver their DNA very efficiently to the nucleus of the invaded cell.[14,15]

The nonviral systems that have been developed so far for gene delivery are characterized by low transfection efficiency compared to the viral delivery vehicles, but are not associated with the significant limitations such as mutagenesis, carcinogenesis, and immune response.[16,17] The most successful nonviral delivery systems used so far are the cationic liposome entrapped DNA and polycation-condensed DNA-type vehicles.[18−21] Although poly(L-lysine)−DNA, a typical vector, can transfer large amounts of genes, it presents low transfection efficiency because DNA is exposed to lysosomal degradation in the intracellular matrix before it approaches the membrane of the nucleus. Liposome-type vectors can better protect their own entrapped DNA; however, a drawback is their limited capability to entrap large amounts of DNA.

We envisioned the amphiphilic triblock copolypeptides of the poly(L-lysine hydrochloride)-b-poly(γ-benzyl-d7-L-glutamate)-b-poly(L-lysine hydrochloride) (PLL-b-PBLG-d7-b-PLL) type with the following desired characteristics: the ability to form vesicles over a wide range of compositions and an efficient virus-like carrier of DNA.

Herein, we provide the first report of the synthesis of well-defined PLL-b-PBLG-d7-b-PLL, using high-vacuum techniques (HVTs) and the sequential ring-opening polymerization (ROP) of the corresponding N-carboxy anhydrides (NCAs) with a difunctional initiator. This synthetic methodology presented recently leads to well-defined triblock and star-block copolypeptides.[22,23] The molecular characteristics of the aggregates formed in water at pH = 7.4 were determined by small-angle neutron scattering (SANS), atomic force microscopy (AFM), static and dynamic light scattering (SLS and DLS), cryo-transmission electron microscopy (cryo-TEM), scanning electron microscopy (SEM), circular dichroism, and UV and Fourier transform infrared (FT-IR) spectroscopy. Vesicular structures were formed in the entire hydrophilic/hydrophobic compositional range of the copolypeptides and were pH/temperature-responsive. It was found that mixtures of plasmid DNA (pDNA) and the triblock copolypeptides also form vesicular structures containing both encapsulated and condensed DNA.

Experimental

A. Polymer Synthesis: Methods and Instrumentation. PLL-b-PBLG-d7-b-PLL triblock amphiphilic copolypeptides were produced from poly(ϵ-Boc-L-lysine)-b-PBLG-d7-b-poly(ϵ-Boc-L-lysine), by selective deprotection of the ϵ-amine group of ϵ-Boc-L-lysine. The precursors were synthesized by the sequential ROP of γ-benzyl-d7-L-glutamate NCA (BLG-d7 NCA) and ϵ-$tert$-butyloxycarbonyl-L-lysine NCA (BLL NCA) with the difunctional initiator 1,6-diaminohexane, using HVTs.[24] It has been shown that the HVT leads to polypeptides with high degrees of molecular and compositional homogeneity. Using this methodology, a series of amphiphilic triblock copolypeptides PLL-b-PBLG-d7-b-PLL having similar molecular weights, but compositions ranging from about 19 to 74% (monomeric units) for the middle block, were synthesized. In the first two copolypeptides, the PLL was held constant, whereas the PBLG-d7 of one was double that of the other. Their solution in water was slightly turbid. In the case of the third copolypeptide, where the water-insoluble block was 74%, the solutions in water were highly turbid. It should be noted that PLL segments are highly charged polyelectrolytes soluble in water, while PBLG-d7, when larger than 80 monomeric units, adopts a regular α-helix conformation insoluble in water.[25]

The protected triblock copolypeptides were excessively characterized by membrane osmometry, size-exclusion chromatography that featured a two-angle laser light scattering detector, (SEC-TALLS), and FT-IR and UV spectroscopy. The molecular characteristics of the polypeptides are given in Table 1. To our knowledge, well-defined orthogonally side chain-protected triblock copolypeptides have not been reported so far. Klok et al. prepared orthogonally protected diblock and random copolypeptides.[26]

DLS measurements were conducted with a Malvern Series 4700. Correlation functions were analyzed by the cumulant method and Contin software. SLS measurements were performed with an Wyatt Dawn Heleos 18-angle detector. AFM measurements were conducted in a heating liquid cell under liquid mode with a Veeco Multimode Nanoscope IIIa. All SANS experiments were performed at 25 °C, in pure D_2O, H_2O, or mixtures of the two, with a KWSII instrument (research reactor FRJ2) at the Forschungszentrum Jülich GmbH. Cryo-TEM images were obtained with an FEI Tecnai 12 instrument operating at a 120 kV accelerating voltage. The vitrified thin films were prepared using an automated FEI Vitrobot system. A Hitachi S-4700 FE-SEM scanning electron microscope was used for direct solution imaging using WetSEM technology. UV spectroscopy was performed with a Perkin-Elmer Lamda 650 spectrometer, from 190 to 500 nm, at room temperature, with cells requiring 120 μL. FT-IR spectroscopy was performed with a Perkin-Elmer Spectrum One spectrometer. Circular dichroism measurements were conducted with a Jasco model J-815-150S.

Details regarding the materials, methods, and instrumentation are provided in the Supporting Information.

B. Preparation of Gene Vehicles. The preparation of the gene vehicles was performed as follows: a solution of the pDNA PUC19, with an initial concentration of ~1000 μg/mL, was further diluted with Milli-Q water until the concentration became 30 μg/mL. Under this dilution, the concentration of the pDNA bases was approximately 8.2×10^{-8} bases/mL. Only the $L_{131}G_{137}L_{131}$ polypeptide was used to form gene vectors. The copolypeptide was dissolved in DMSO, and its concentration was adjusted to that of the pDNA base solution. The mixtures of copolypeptides and pDNA were performed by slowly adding the pDNA solution to the appropriate solution of polypeptides.

Table 2. DLS Measurements at pH = 7.4, 25 °C, and 90°

sample	R_H (nm)
$L_{134}G_{64}L_{134}$	129 ± 6.8
$L_{131}G_{137}L_{131}$	135 ± 7.5
$L_{64}G_{181}L_{64}$	145 ± 8.2

Table 3. SLS Results at pH = 7.4 and 25 °C

| sample	R_G (nm)	R_G/R_H	$M_{w\ ap} \times 10^{-6}$	N_{ap}	A_{ap} (nm²)
$L_{134}G_{64}L_{134}$	131 ± 8.9	1.02	186 ± 5.6	3195	65
$L_{131}G_{137}L_{131}$	137 ± 4.5	1.01	207 ± 4.5	2797	81
$L_{64}G_{181}L_{64}$					

Thus, the polypeptides were not aggregated, and the PLL could interact with the genes. The mixture was left to shake for 3 days, immersed in the membrane, and finally was exhaustively dialyzed against Milli-Q water.

Results and Discussion

DLS. There was no indication of the presence of unimers from Contin analysis in the concentration range studied for all samples. The polydispersity of the aggregates derived from cumulant analysis was <0.15 for all angles and concentrations in the cases of $L_{131}G_{137}L_{131}$ and $L_{134}G_{64}L_{134}$ and was <0.3 for $L_{64}G_{181}L_{64}$. There was insignificant (<5%) angular/concentration dependence of the diffusion constant and consequently of the hydrodynamic radii (R_H), indicating that the sample was isotropic and spherical. Moreover, the R_H was almost constant (<5%) upon increasing the temperature to 50 °C. The hydrodynamic radii obtained at 90° are shown in Table 2, indicating the formation of large aggregates. Since the size of a single polypeptide molecule is expected to be less than 30 nm,[27,28] large spherical aggregates can only be formed if they are hollow.

SLS. The results of the SLS are shown in Table 3. The obtained values of the radius of gyration (R_G), the ratios of R_G/R_H, along with the apparent weight average molecular weights, the apparent aggregation number, and the surface occupied by each PLL chain are provided. The values of the R_G/R_H ratios for $L_{134}G_{64}L_{134}$ and $L_{131}G_{137}L_{131}$ are close to unity, as theoretically expected for a hollow sphere. In the case of uniform spheres or random coils, the expected corresponding values are 0.774 and 1.50.[29] The apparent aggregation number obtained was rather low for such large aggregates. The surface area values of 65 and 81 nm² for each polymeric chain are rather large compared to the surface of the cylinder end of an α-helical PBLG (πr^2, where r is the radius of the cylinder) ranging from 1.9 to 5.3 nm², depending on the conformation of the benzyl group.[30] This difference could be due either to the underestimation of the molecular weight of the aggregates, and therefore of the aggregation number, or to the slanted orientation of the cylinders along the monolayer. Due to the low concentrations used, there might be unimers in the system, which would result in underestimation of the molecular weight of the aggregates.

AFM. The vesicular structures of the aggregates were confirmed using AFM. Representative height images of the aggregates are shown in Figure 1. It was found that the operation under liquid mode was very sensitive to the type of tips and to the concentration of the solution. A significant amount of destroyed vesicles was found on the surface of the glass substrate, with height on the order of 4−4.5 nm. In many cases, in our effort to break the aggregates, the structures were split into two smaller spherical structures.
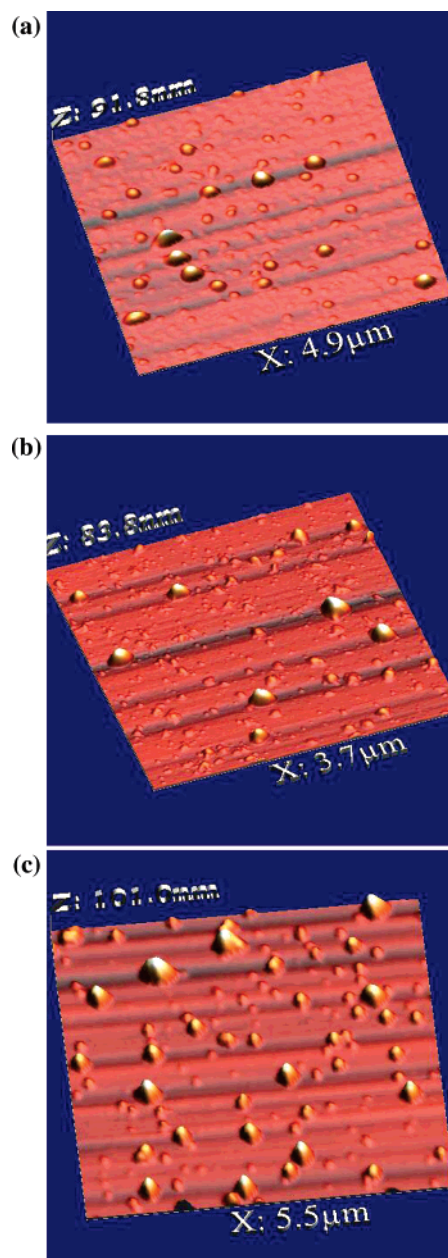
Figure 1. Typical height images of the copolypeptides (a) $L_{134}G_{64}L_{134}$, (b) $L_{131}G_{137}L_{131}$, and (c) $L_{64}G_{181}L_{64}$.

Therefore, small structures having heights less than 4 nm, randomly distributed on the surface of the glass, were inevitable and were considered noise in the presence of the larger structures.

The results obtained from the AFM images concerning the form, polydispersity, and dimensions of the aggregates are in excellent agreement with those obtained by DLS. The structures in the case of the first two copolypeptides present low polydispersity and a diameter of about 250 nm, whereas higher polydispersity and dimensions were observed for the third copolypeptide with the highest insoluble block.

One indication of the vesicular structures is the image of the phase as compared to that of the height. The height image of a typical spherical structure is shown in Figure 2a, and the corresponding phase image is shown in Figure 2b. Since the phase depends on the energy that dissipates from the structures to the tip, higher values correspond to harder structures. Therefore, from the phase picture it can be concluded that the structure is harder in the outer periphery than in the middle
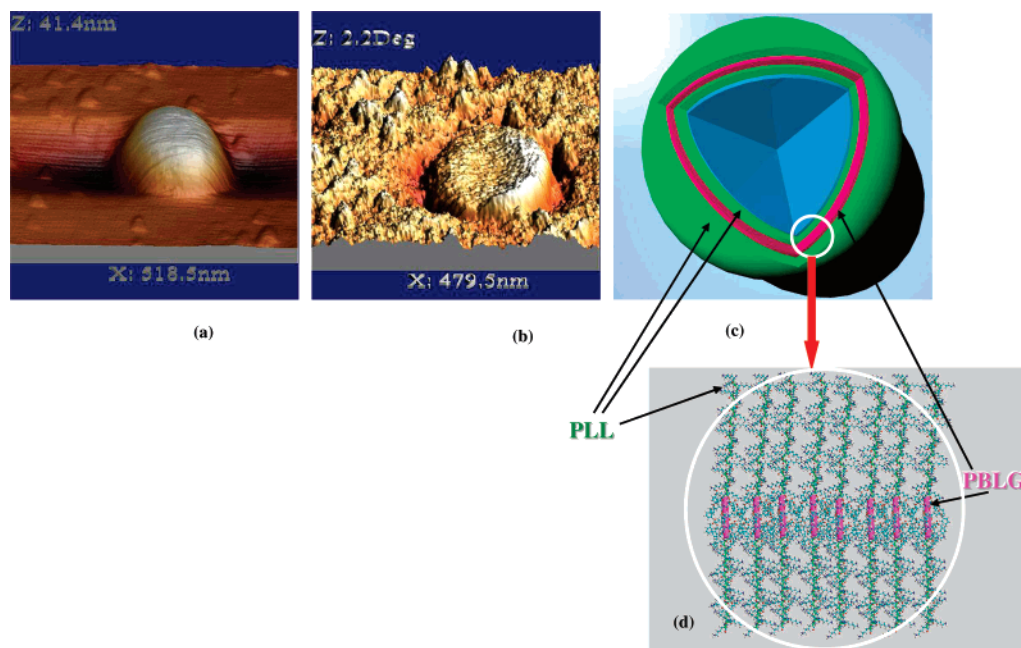
Figure 2. (a) Typical height image of the structures observed from the $L_{134}G_{64}L_{134}$ copolypeptide; (b) the corresponding phase image of the same structure shown in panel a; (c) schematic representation of a vesicular structure; (d) schematic representation of the membrane.
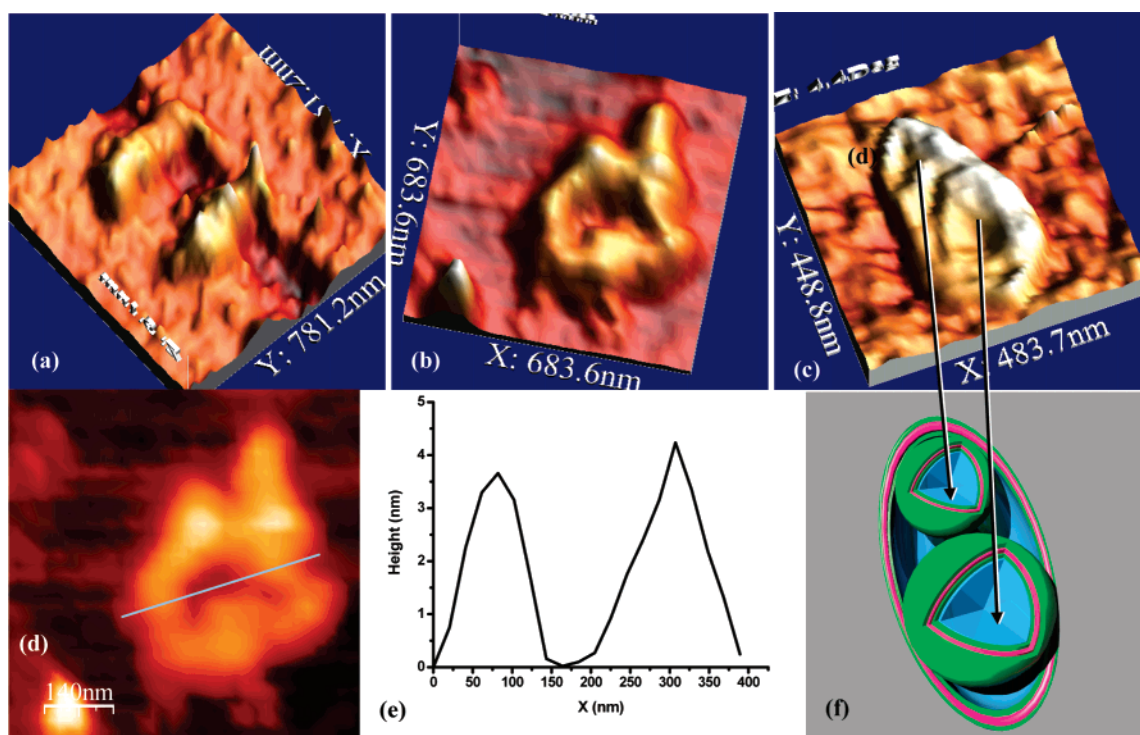

Figure 3. Typical 3D height image of a disrupted vesicle of the copolypeptides (a) $L_{134}G_{64}L_{134}$ and (b) $L_{131}G_{137}L_{131}$, after rupture of the vesicle monolayer. (c) Typical phase picture of the vesicular structures obtained by the copolypeptide $L_{64}G_{181}L_{64}$. (d) The 2D image representation of panel b. (e) The height profile along the line shown in panel (d). (f) The schematic representation of panel c.

part due to the water contained in the vesicle, rendering the surface of the vesicle softer on the interior than on the exterior.

The formation of vesicular structures was also supported after disruption of the spherical aggregates (Figure 3). In Figure 3a,b, the ruptured vesicles of the $L_{134}G_{64}L_{134}$ and $L_{131}G_{137}L_{131}$ copolypeptides are shown. It was found that, in the case of the first copolypeptides, with the lowest insoluble block, the vesicles were rather sensitive and the structures were easily disrupted (Figure 3a).The vesicles of the second copolypeptide were less sensitive and, when ruptured, gave the typical image of a hollow

sphere (Figure 3b). A two-dimensional (2D) representation of Figure 3b is provided in Figure 3d. The height profile along the line of the ruptured vesicle of Figure 3d is shown in Figure 3e. The height of the disrupted monolayer was always less than 4.5 nm. The width of the collapsed membranes was approximately 150 nm (Figure 3e) for the two copolypeptides with a smaller amount of the insoluble block.

The space occupied by the collapsed monolayers on the glass substrate is significantly larger than that of the vesicle membrane in solution, and direct comparison of the dimensions cannot be
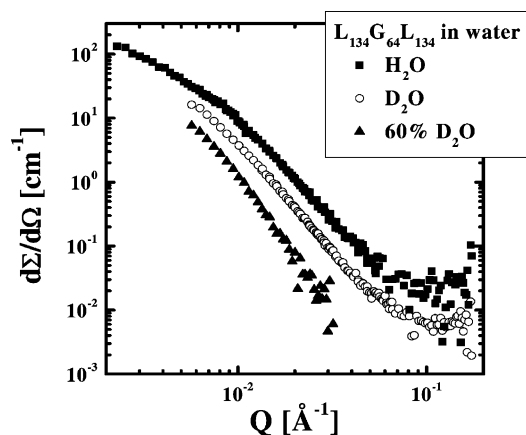
Figure 4. Scattering cross section of the vesicle-forming polymer $L_{131}G_{64}L_{131}$ in water with different contrasts.

made. In the case of the third copolypeptides, with the highest proportion of the insoluble block, the structures were more robust and could not be broken with the cantilevers used.

The vesicular form was confirmed by the phase image of the AFM measurements. In the phase image of a typical vesicle of $L_{64}G_{181}L_{64}$ (Figure 3c) it can be seen that the species are composed of two smaller vesicles inside a larger one. The schematic representation of the structure is shown in Figure 3f.

SANS Results. We performed contrast variation measurements of the three copolypeptides by varying the scattering length density of the water by the addition of D_2O. A representative example for $L_{131}G_{64}L_{131}$ is given in Figure 4. The scattering profile depicted is typical of a spherical structure. The size of the vesicular structures was too large for the Q range measured by the instrument. Nevertheless, the intermediate Q range measured (0.007–0.04 Å^{-1}) was sufficient to draw conclusions concerning the compactness of the vesicles.

In order to determine the compactness of the vesicles, it was necessary to obtain the scattering length density (SLD) of the two blocks. Their experimentally obtained contrast matches could be simply explained by the calculated scattering length densities of the individual PBLG-d7 midblock and the PLL brushes, but only if we assume that the PBLG-d7 exchanges two hydrogens with the deuterium of D_2O, and PLL exchanges five. Furthermore, the PLL is assumed to bind five water molecules through hydrogen bonding: three with the ϵ-amine group, one with the amidic H, and one with the C=O group. The water molecules attached to the PLL block represent the so-called "hydration shell" found by SANS on natural peptides,[31] which significantly increases the overall dimensions of the molecules. After considering these factors, contrast matches with densities of 1.31 and 1.12 g/cm^3 were obtained for PBLG-d7 and PLL, respectively. The dependence of the SLD on the $D_2O\%$ in the D_2O/H_2O mixtures is illustrated in Figure 5a.

Since only the intermediate Q range was measured, we tried to extract a power law at the scattering vector $Q = 0.01$ Å^{-1} to reveal the degree of compactness of the vesicles. In Figure 5b, the exponent α is a function of the D_2O content for the three different polymers. In pure H_2O, almost surface-like scattering is observed for $L_{131}G_{64}L_{131}$, whereas $L_{131}G_{137}L_{131}$ lies in the intermediate range (semi-compact), and $L_{64}G_{181}L_{64}$ is compact (filled). This is in agreement with the AFM images, where the vesicles of $L_{64}G_{181}L_{64}$ were intrinsically structured, that is, two or three vesicles were included in a larger one, rendering the overall vesicle compact. At high D_2O contents, a slightly lower exponent was found compared to the initial H_2O value. In particular, the deviations at the contrast match are interesting
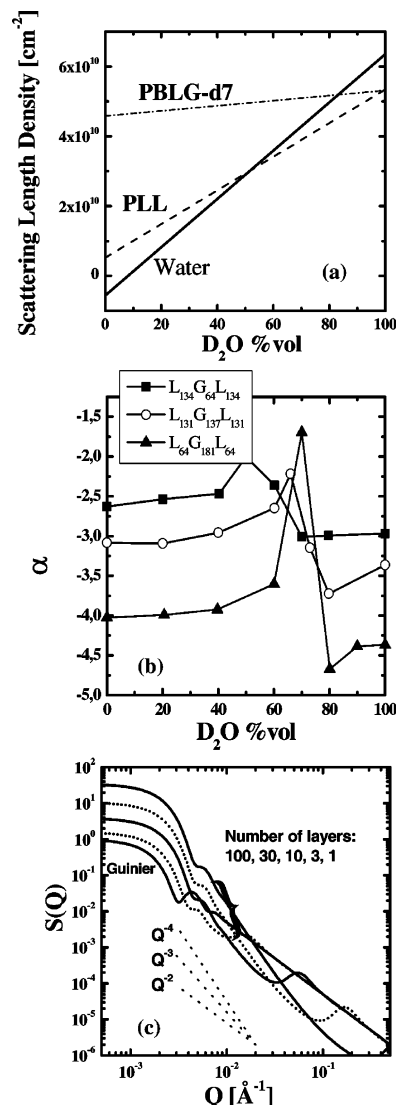

Figure 5. (a) The SLDs as determined from the contrast variation experiment. Due to hydrogen exchange, the polymer SLD changes with the D_2O content, (b) Exponent α determined as a slope in a log–log plot of the scattering intensity (such as panel a). The closer α is to −2, the more open the structure is. The closer α is to −4, the more compact the structure is. So α is a measure of compactness. (c) Theoretical scattering model calculations for multilamellar vesicles with different numbers of layers. For simplicity, the outer radius $R = 1000$ Å was kept constant. A 15% smearing of the intensities was allowed to simulate polydispersity and instrument resolution. This model should demonstrate how the compactness can be read from slopes of the scattering intensity.

and can be explained by the kinetically slow exchange of the included water. During the preparation of the samples, the D_2O content was simply changed by adding a certain amount of H_2O/D_2O mixtures to the stock solution. The solvent exchange from the interior to the exterior of the vesicles was kinetically slow, and thus an additional contrast from the filled vesicle interior part to the external solvent is created. This exchange is slower for the more compact multilamellar vesicles compared to the simple ones, and thus, the $L_{64}G_{181}L_{64}$ polymer shows the greatest contrast at the matching point.

We developed a model for isolated multilamellar vesicles, in order to relate α with the compactness. Here we assume, for a given overall size R and varying number N of inner lamellae, exactly concentric spherical shells ($i = 1...N$), with radii of $r = R \cdot i/N$, and infinitely thin shells. The resulting formula is as follows:

$$S(q = QR/N) =$$

$$\frac{3}{N^3\left(N+\frac{1}{2}\right)(N+1)}\left(-\frac{1}{2}\cos\left(q\left(N+\frac{1}{2}\right)\right)\left(N+\frac{1}{2}\right) + \right.$$

$$\left.\frac{1}{4}\sin\left(q\left(N+\frac{1}{2}\right)\right)/\tan\left(\frac{1}{2}q\right)\right)^2/\left(q\sin\left(\frac{1}{2}q\right)\right)^2$$

The graphical representation is shown in Figure 5c. The radius was chosen as $R = 1000$ Å, and the number of shells was chosen as 1, 3, 10, 30, and 100. At the middle Q range, a power-law region appears, which reveals the compactness of the vesicle and raises upon increasing the number of shells from Q^{-2} for surfaces to Q^{-4} for compact spheres.

This simple model explains how the compactness of the vesicles appears in the measured SANS spectra. The deviations from the experimental SANS results are due to the assumption of infinitely thin and concentric spherical shells. In the formed vesicles, depending on the composition of the copolypeptide, the thickness of the monolayer is expected to be from 10 to 30 nm.[27,28] In the case of $L_{64}G_{181}L_{64}$, nonconcentric vesicles were observed by AFM and consequently smeared out any peak predicted by the model.

Consequently, the model supports the experimentally obtained increase in α, which could be due either to the increased thickness of the membrane (in the case of the first two polymers) or to the formation of highly structured vesicles.

Cryo-TEM and SEM. As an example, a typical TEM image of the vesicular structures formed by $L_{131}G_{137}L_{131}$ in water is shown in Figure 6a. The RuO$_4$-stained PBLG-d7 block can be seen on the outer periphery of the vesicular structure (indicated by the arrow). Moreover, the size ($\sim$250 nm) is in agreement with the one obtained by SLS and AFM measurements. Similar results were obtained by SEM (Figure 6b).

Moreover, the polydispersity of the aggregates is relatively low, in agreement with the DLS measurements. Similar images were obtained for the aggregates of $L_{134}G_{64}L_{134}$. Unfortunately, it was not possible to obtain reliable images for $L_{64}G_{181}L_{64}$, because crystallization of the insoluble block was induced.

Stimuli-Responsive Effect to pH and Temperature. It is well established that polylysine adopts the random coil conformation at pH = 7.4, whereas it becomes an α-helix at pH = 11.5. When the temperature is raised while the pH is maintained at 11.5, PLL is transformed to a β-sheet.[32] The temperature at which this transition occurs depends on the molecular weight: the higher the molecular weight, the lower the temperature. For a molecular weight of approximately 20×10^3 g/mol (as in the case of $L_{134}G_{64}L_{134}$ and $L_{131}G_{137}L_{131}$), at 37 °C, more than 90% of the chains are transformed from the α-helix to a β-sheet. For lower molecular weight values ($\sim$10 $\times$ 10^{3}g/mL), at 37 °C, less than 5% of the chains adopt the β-sheet conformation (as in the case of $L_{64}G_{181}L_{64}$).[32]

Samples of the solutions of the three copolypeptides initially measured at pH = 7.4, were brought to pH = 11.7 upon the addition of a concentrated solution of NaOH, and were subsequently measured by DLS at various angles, at 25 °C. As in the case of the aggregates at pH = 7.4, no dependence of the hydrodynamic radius on the angle or concentration was observed, and only one population of aggregates was present in the solution. The R_H values (Table 4) were significantly lower than those found at pH = 7.4 (Table 2). The molecular weight of the aggregates was monitored by SLS, and was found to be identical to that at pH = 7.4. Although the PBLG-d7 block is not sensitive to any pH or temperature change, the lower values obtained for the R_H are due to the reduced dimensions of the
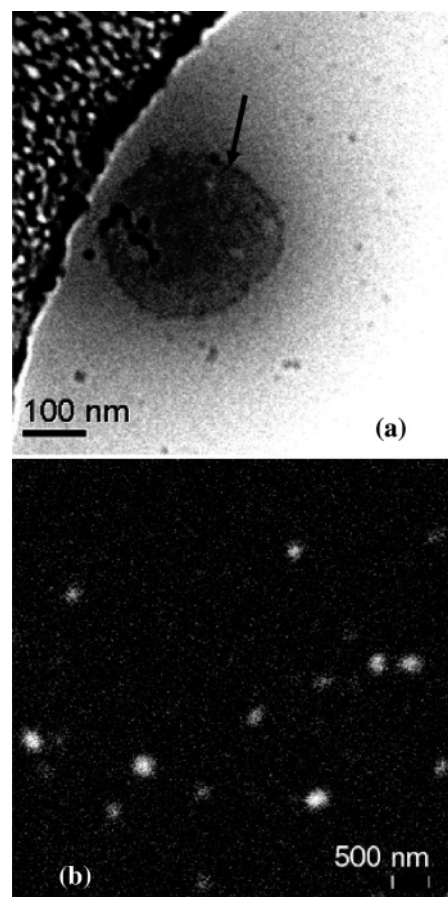

Figure 6. Cryo-TEM (a) and SEM (b) of the aggregates of $L_{131}G_{137}L_{131}$ formed in water at pH = 7.4.

Table 4. DLS Measurements at 90°

	R_H (nm)	
sample	25 °C, pH = 11.7	37 °C, pH = 11.7
$L_{134}G_{64}L_{134}$	92.5	148
$L_{131}G_{137}L_{131}$	105	135
$L_{64}G_{181}L_{64}$	117.5	117.5

polylysine block.[32] Therefore, under these conditions, PLL is transformed from the extended random coil to the compact α-helical conformation (Figure 7).

The same solutions were immersed in a bath at 37 °C, for 4 h, and were then analyzed by DLS. The sizes of the vesicles were higher than those of the vesicles at pH = 7.4 and 25 °C. This is due to the transition of the PLL to the β-sheet conformation, which is significantly elongated in comparison to the helical form (Figure 7).

In the case of $L_{64}G_{181}L_{64}$, due to the low molecular weight of the PLL block, the vesicle sizes were not changed, as expected.

The secondary structure of the different blocks was obtained by circular dichroism (Figure 8). The spectra obtained under different conditions were the sum of the spectra of the insoluble PBLG-d7 and that of the PLL block. The spectra of the PBLG-d7 suspension is attributed to an aggregated α-helix form.[33] The spectra from the PBLG part was subtracted for the visualization of the PLL blocks.

The circular dichroism spectra confirm, on one hand, that the PBLG-d7 block remains as it is in solid state, and, on the other hand, that the PLL block adopts the same secondary structure as that of the homopolymer, depending on the pH.
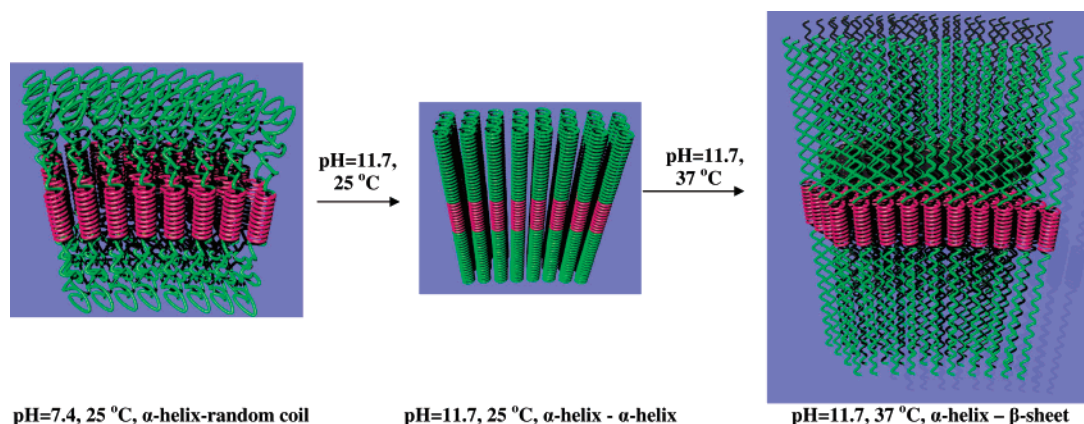
pH=7.4, 25 °C, α-helix-random coil   pH=11.7, 25 °C, α-helix - α-helix   pH=11.7, 37 °C, α-helix – β-sheet

Figure 7. Schematic representation of the influence of the pH and temperature on the dimensions of the monolayer and, consequently, of the vesicle: (a) pH = 7.4, 25 °C, the PLL block has a random coil conformation; (b) pH = 11.7, 25 °C, the PLL block has an α-helix conformation; (c) pH = 11.7, 37 °C, the PLL block has a β-sheet conformation. In all cases, the PBLG-d7 block has an α-helix conformation.
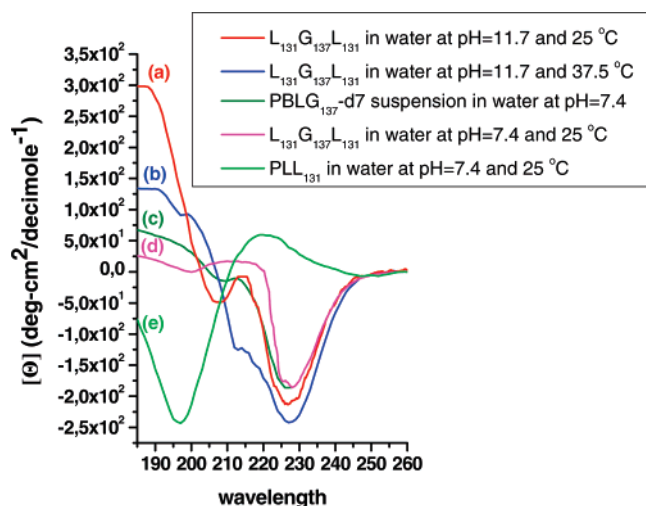

Figure 8. Circular dichroism spectra of (a) $L_{131}G_{137}L_{131}$ in water at pH = 11.7 and 25 °C, (b) $L_{131}G_{137}L_{131}$ in water at pH = 11.7 and 37.5 °C, (c) $PBLG_{137}$-d7 suspension in water at pH = 7.4, (d) $L_{131}G_{137}L_{131}$ suspension in water at pH = 7.4 and 25 °C, and (e) PLL_{131} in water at pH = 7.4, at 25 °C.

Table 5. DLS Measurements of the Vectors at pH = 7.4, 25 °C, and 90°

$L_{131}G_{137}L_{131}$/Puc19	R_H (nm)
3/2	390
1/1	320

Polypeptide−DNA Vectors. In dimethyl sulfoxide (DMSO), the copolypeptides are not aggregated, thus the PLL can interact with the genes when the solutions of the two components are combined. The pDNA is expected to condense onto the PLL block through electrostatic interactions and be encapsulated in the vesicular structures formed. Two different ratios of PLL over pDNA bases (PLL/pDNA)—3:2 and 1:1—were used.

The quantitative condensation/encapsulation of the pDNA was monitored by UV spectroscopy. The free DNA absorbs strongly at 260 nm, whereas, after condensation, the pDNA-copolypeptide vector absorbs at 206 nm. The molecular characteristics of the vectors were obtained by DLS, AFM, and UV spectroscopy. The DLS results are provided in Table 5. It was found that the vectors became more compact upon increasing the amount of pDNA.

The polydispersity of the formed vectors was high and the angular independence of R_H implies the spherical structure of the aggregates.

The vesicular structure of the aggregates was verified by AFM. A typical 3D height image of the aggregates of $L_{131}G_{137}L_{131}$ with pDNA (charge ratio of 1:1) is shown in Figure 9a.

In this image, most of the vesicles have been disrupted, while some are still intact. The diameters of the intact vesicular structures were similar to those obtained by DLS, that is, about 320 nm.

Most of the ruptured aggregates were empty in the center, indicating their vesicular structure. The ruptured vesicles that appear to be filled are the result of the presence of pDNA. The magnification of a disrupted vesicle is depicted in Figure 9b. Figure 9d is the 2D representation of this image, while the height profile along the line in Figure 9d is shown in Figure 9e. It is clear that the space occupied (both height and width) by the collapsed membranes ($L_{131}G_{137}L_{131}$) increased significantly to about 400 nm (width) and 6.0−6.5 nm (height, Figure 9e), as compared to that of the corresponding collapsed monolayers not containing the genes (Figure 3b). This increase is clearly due to the complexation/encapsulation of the pDNA. The position of the condensed pDNA was verified by examination of the phase image of the ruptured vesicles (Figure 9c). It was found that the inner and outer peripheries of the collapsed membrane, (shown as yellow areas), are more rigid due to the condensed pDNA on the PLL phase (Figure 9c). This is also supported by the phase image of the disrupted $L_{131}G_{137}L_{131}$ vesicle not containing the genes, which was homogeneous, since all the species were polypeptides with similar rigidity (Figure 9g).

Inside every collapsed monolayer there are globular species with heights of about 12 nm, which do not appear for those vesicles without pDNA. These species correspond to the encapsulated free pDNA, which exists inside the vesicle. By disrupting the vesicle, the collapsed monolayers drag the encapsulated pDNA molecules, which are then entrapped on the substrate. The free pDNA in water does not interact with the glass substrate, so it cannot be seen by AFM. Unfortunately, the standard mica or highly oriented pyrolythic graphite (HOPG) methodology used to examine DNA species could not be applied because the vesicles were randomly ruptured upon reaching the surface of the mica.[34] However, with a glass substrate, controlled rupturing of the vesicles was achieved, leading to the immobilization and visualization of both condensed and globular (encapsulated) pDNA.

There are some reports on the synthesis of polymeric hollow capsules for drug or gene delivery.[35−37] It has recently been
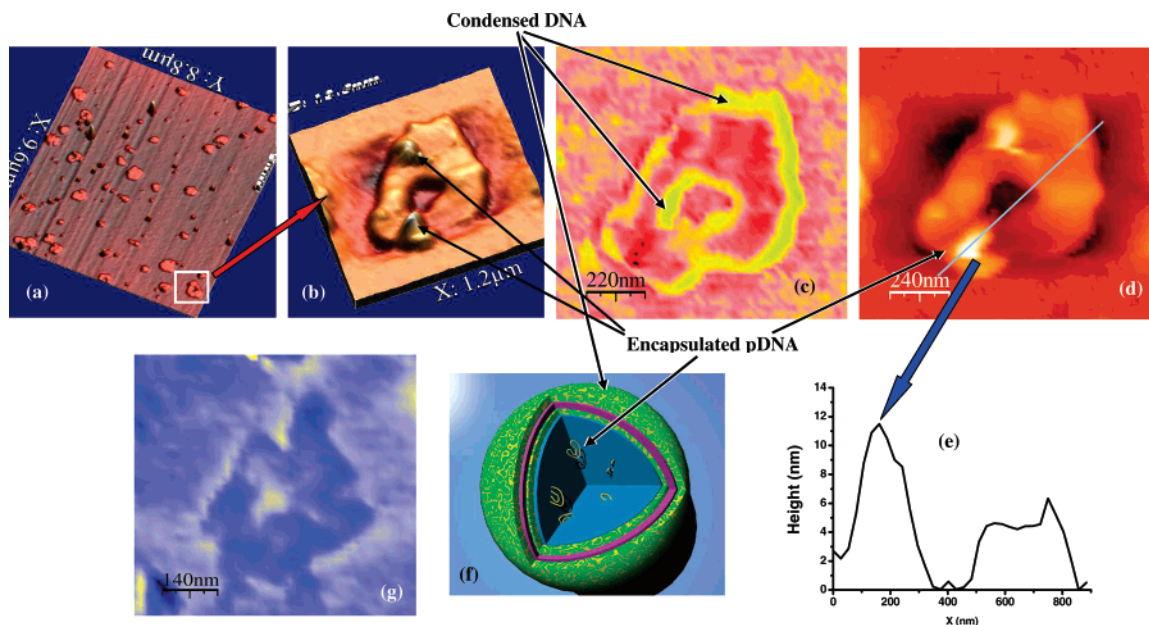
Figure 9. (a) Typical 3D height picture of a disrupted vesicle of the mixtures of the copolypeptide $L_{134}G_{64}L_{134}$ with the pDNA PUC19. (b) Magnification of the 3D height picture of a ruptured vesicle. (c) The phase image of panel b. (d) The 2D height picture of panel c. (e) The height profile along the line in panel d. (f) Schematic representation of the encapsulated and condensed pDNA on the vesicular structure. (g) Phase picture of the ruptured vesicle of the copolypeptide $L_{134}G_{64}L_{134}$, without the pDNA.

found that, when PLL homopolypeptide is mixed with plasmid genes, the resulting condensates have a toroid form, due to the increase in rigidity of the PLL block when oppositely charged molecules condense on it.[38−39] In the case of the triblock copolypeptides, although the rigidity of the PLL block increased with the condensation of pDNA, the hydrophobic interactions still dominated and forced the overall system to form vesicular structures.

In summary, a series of partially labeled amphiphilic triblock copolypeptides, PLL-*b*-PBLG-d7-*b*-PLL, have been synthesized using HVT, a diamino initiator, and the sequential ROP of BLG-d7 NCA and BLL NCA, followed by the selective deprotection of the Boc groups. The triblock copolypeptides had similar molecular weights, but different compositions, and high degrees of molecular/compositional homogeneity. The aggregates formed in water were excessively characterized by SLS and DLS, SANS, AFM, cryo-TEM, UV and FT-IR spectroscopy, as well as circular dichroism. The formation of hollow spherical aggregates was favored, and vesicular structures were formed in all compositions. This is due to (a) the rigid middle block of the copolypeptide, which prevents the chains from bending, (b) the macromolecular architecture, which forms a monolayer more readily than the corresponding diblock copolypeptides that must adopt an antiparallel orientation to form a bilayer, and (c) similar curvature induced by the equal PLL blocks, which promotes the formation of planar monolayers rather than micelles.

Compared to other vesicular structures formed by conventional amphiphilic copolymers, our vesicles possess the unique feature of being stimuli-responsive to pH and temperature. Another unique feature of these vesicles is the tunable thickness of the monolayer, along with their thermodynamic preference to adopt and maintain the vesicular structure. Consequently, they are expected to be stable in different environments, making them appropriate materials for the encapsulation and protection of drugs or genes. The pH response of polylysine is indeed outside the physiological range. Nevertheless, the results are very interesting and can serve as a model for similar copolypeptides containing, for example, polyhistidine, which is responsive at pH = ∼6.15.[40] By mixing amphiphilic triblock copolypeptides

with pDNA, larger vesicular structures are formed. The pDNA is partially condensed on the PLL phase, and partially encapsulated inside the vesicle, mimicking the viral counterpart.

Supporting Information Available. Details regarding the experimental materials, methods, and instrumentation. This material is available free of charge via the Internet at http://pubs.acs.org.

Note Added after ASAP Publication. This article was released ASAP on June 21, 2007 without the Supporting Information description paragraph. The corrected version which includes the paragraph posted on June 28, 2007.

References and Notes

(1) Discher, D.; Eisenberg, A. *Science* **2002**, *297*, 967−973.
(2) Ahmed, F.; Photos, P.; Discher, D. E. *Drug Dev. Res.* **2006**, *67*, 4−14.
(3) Putnam, D. *Nat. Mater.* **2006**, *5*, 439−451.
(4) Luo, D.; Saltzman, W. *Nat. Biotechnol.* **2000**, *18*, 33−37.
(5) Merdan, T.; Kopeček, J.; Kissel, T. *Adv. Drug Delivery Rev.* **2002**, *54*, 715−758.
(6) (a) Yu, K.; Eisenberg, A. *Macromolecules* **1998**, *31*, 3509−3518. (b) Luo, L.; Eisenberg, A. *Langmuir* **2001**, *17*, 6804−6811.
(7) Cornelissen, J. J. L. M.; Fischer, M.; Sommerdijk, N. A. J. M.; Nolte, R. J. M. *Science* **1998**, *280*, 1427−1430.
(8) Kukula, H.; Schlaad, H.; Antonietti, M.; Förster, S. *J. Am. Chem. Soc.* **2001**, *124*, 1658−1663.
(9) Chécot, F.; Lecommandoux, S.; Gnanou, Y.; Klok, H.-A. *Angew. Chem., Int. Ed.* **2002**, *41*, 1340−1343.
(10) Chécot, F.; Brûlet, A.; Oberdisse, J.; Gnanou, Y.; Mondain-Monval, O.; Lecommandoux, S. *Langmuir* **2005**, *21*, 4308−4315.
(11) Holowka, E.; Pochan, D.; Deming, T. *J. Am. Chem. Soc.* **2005**, *127*, 12423−12428.
(12) Rodriguez-Hernández, J.; Lecommandoux, S. *J. Am. Chem. Soc.* **2005**, *127*, 2026−2027.
(13) Bellomo, E.; Wystra, M.; Paktsis, L.; Pochan, D.; Deming, T. *Nat. Mater.* **2004**, *3*, 244−248.
(14) Stull, R. A.; Szoka, F. C. *Pharm. Res.* **1995**, *12*, 465−483.
(15) Pastil, S. D.; Burgess, D. J. *AAPS Newsmagazine* **2003**, *6*, 27.
(16) Schaltzlein, A. G. *Anti-Cancer Drugs* **2001**, *12*, 275−304.

(17) Vijayanathan, V.; Thomas, J.; Thomas, J. T. *Biochemistry* **2002**, *41*, 14085−14094.

(18) Meyer, M.; Wagner, E. *Hum. Gene Ther.* **2006**, *17* (11), 1062−1076.

(19) Zauner, W.; Orgis, M.; Wagner, E. *Adv. Drug Delivery Rev.* **1998**, *30*, 97−113.

(20) Park, G.; Hoon Jeong, J.; Wan Kim, S. *Adv. Drug Delivery Rev.* **2006**, *58*, 467−486.

(21) Kabanov, A. V.; Kabanov, V. A. *Bioconjugate Chem.* **1995**, *6*, 7−20.

(22) Aliferis, T.; Iatrou, H.; Hadjichristidis, N. *Biomacromolecules* **2004**, *5*, 1653−1656.

(23) Aliferis, T.; Iatrou, H.; Hadjichristidis, N. *J. Polym. Sci., Part A.: Polym. Chem*. **2005**, *43*, 4670−4673.

(24) Hadjichristidis, N.; Iatrou, H.; Pispas, S.; Pitsikalis, M. *J. Polym. Sci., Part A.: Polym. Chem.* **2000**, *38*, 3211.

(25) Lecommandoux, S.; Achard, M.; Langewalter, J.; Klok, H. *Macromolecules* **2001**, *34*, 9100−9111.

(26) Rodríguez Hernández, J.; Klok, H. *J. Polym. Sci., Part A.: Polym. Chem.* **2002**, *41*, 1167−1187.

(27) Lübbert, A.; Castelletto, V.; Hamley, I.; Nuhn, H.; Scholl, M.; Bourdillon, L.; Wandrey, C.; Klok, H. *Langmuir* **2005**, *21*, 6582−6589.

(28) Papadopoulos, P.; Floudas, G.; Schnell, I.; Aliferis, T.; Iatrou, H.; Hadjichristidis, N. *Biomacromolecules* **2005**, *6*, 2352−2361.

(29) Burchard, W. *Adv. Polym. Sci.* **1983**, *48*, 1−124.

(30) Chang, Y.; Frank, C. *Langmuir* **1996**, *12*, 5824−5829.

(31) Weik, M.; Lehnert, U.; Zaccai, G. *Biophys. J.* **2005**, *89*, 3639−3646.

(32) Dzwolak, W.; Muraki, T.; Kato, M.; Taniguchi, T. *Biopolymers* **2004**, *73*, 463−469.

(33) Cho, C.; Nah, J.; Jeong, Y.; Cheon, J.; Asayama, S.; Ise, H.; Akaike, T. *Polymer* **1999**, *40*, 6769−6775.

(34) Yang, W.; Hwang, S.; Chen, F.; Chang, S.; Tsai, P. *Nanotechnology* **2007**, *18* (8), article no. 084009.

(35) Zelikin, A.; Quinn, J.; Caruso, F. *Biomacromolecules* **2006**, *7*, 27−30.

(36) Haynie, D.; Palath, N.; Liu, Y.; Li, B.; Pargaonkar, N. *Langmuir* **2005**, *21*, 1136−1138.

(37) Shchukin, D.; Patel, A.; Sukhorukov, G.; Lvov, Y. *J. Am. Chem. Soc.* **2004**, *126*, 3374−3375.

(38) Tang, M.; Li, W.; Szoka, F. *J. Gene Med.* **2005**, *7*, 334−342.

(39) Golan, R.; Pientrasanta, L.; Hsieh, W.; Hasma, H. *Biochemistry* **1999**, *38*, 14069−14076.

(40) Patchornik, A.; Berger, A.; Katchalski, E. *J. Am. Chem. Soc.* **1957**, *79*, 5227−5230.